Eur J Nucl Med Mol Imaging (2016) 43:1323–1336
DOI 10.1007/s00259-016-3309-5

ORIGINAL ARTICLE

Reduction in camera-specific variability in [^{123}I]FP-CIT SPECT outcome measures by image reconstruction optimized for multisite settings: impact on age-dependence of the specific binding ratio in the ENC-DAT database of healthy controls

Ralph Buchert[1] · Andreas Kluge[2] · Livia Tossici-Bolt[3] · John Dickson[4] · Marcus Bronzel[2] · Catharina Lange[1] · Susanne Asenbaum[5] · Jan Booij[6] · L. Özlem Atay Kapucu[7] · Claus Svarer[8] · Pierre-Malick Koulibaly[9] · Flavio Nobili[10] · Marco Pagani[11,12] · Osama Sabri[13] · Terez Sera[14] · Klaus Tatsch[15] · Thierry Vander Borght[16] · Koen Van Laere[17] · Andrea Varrone[18] · Hidehiro Iida[19]

Received: 18 September 2015 / Accepted: 5 January 2016 / Published online: 27 January 2016

Abstract

Purpose Quantitative estimates of dopamine transporter availability, determined with [^{123}I]FP-CIT SPECT, depend on the SPECT equipment, including both hardware and (reconstruction) software, which limits their use in multicentre research and clinical routine. This study tested a dedicated reconstruction algorithm for its ability to reduce camera-specific intersubject variability in [^{123}I]FP-CIT SPECT. The secondary aim was to evaluate binding in whole brain (excluding striatum) as a reference for quantitative analysis.

Methods Of 73 healthy subjects from the European Normal Control Database of [^{123}I]FP-CIT recruited at six centres, 70

Ralph Buchert and Andreas Kluge contributed equally to this work.

✉ Ralph Buchert
ralph.buchert@charite.de

1 Department of Nuclear Medicine, Charité – Universitätsmedizin Berlin, Berlin, Germany

2 ABX-CRO advanced pharmaceutical services Forschungsgesellschaft m.b.H., Dresden, Germany

3 Department of Medical Physics, University Hospital Southampton NHS Foundation Trust, Southampton, UK

4 Institute of Nuclear Medicine, University College London Hospital NHS Foundation Trust, London, UK

5 Department of Nuclear Medicine, Medical University of Vienna, Vienna, Austria

6 Department of Nuclear Medicine, Academic Medical Centre, University of Amsterdam, Amsterdam, The Netherlands

7 Department of Nuclear Medicine, Faculty of Medicine, Gazi University, Ankara, Turkey

8 Neurobiology Research Unit, Rigshospitalet and University of Copenhagen, Copenhagen, Denmark

9 Nuclear Medicine Department, Centre Antoine Lacassagne, University of Nice-Sophia Antipolis, Nice, France

10 Department of Neuroscience (DINOGMI), Clinical Neurology Unit, University of Genoa, Genoa, Italy

11 Institute of Cognitive Sciences and Technologies, CNR, Rome, Italy

12 Department of Nuclear Medicine, Karolinska Hospital, Stockholm, Sweden

13 Department of Nuclear Medicine, University of Leipzig, Leipzig, Germany

14 Department of Nuclear Medicine and Euromedic Szeged, University of Szeged, Szeged, Hungary

15 Department of Nuclear Medicine, Municipal Hospital of Karlsruhe Inc, Karlsruhe, Germany

16 Nuclear Medicine Division, Université catholique de Louvain, CHU Namur, IREC, Yvoir, Belgium

17 Nuclear Medicine, University Hospital and K.U. Leuven, Leuven, Belgium

18 Department of Clinical Neuroscience, Centre for Psychiatry Research, Karolinska Institutet, Karolinska University Hospital, Stockholm, Sweden

19 National Cerebral and Cardiovascular Center – Research Institute, Osaka, Japan

aged between 20 and 82 years were included. SPECT images were reconstructed using the QSPECT software package which provides fully automated detection of the outer contour of the head, camera-specific correction for scatter and septal penetration by transmission-dependent convolution subtraction, iterative OSEM reconstruction including attenuation correction, and camera-specific "to kBq/ml" calibration. LINK and HERMES reconstruction were used for head-to-head comparison. The specific striatal [^{123}I]FP-CIT binding ratio (SBR) was computed using the Southampton method with binding in the whole brain, occipital cortex or cerebellum as the reference. The correlation between SBR and age was used as the primary quality measure.

Results The fraction of SBR variability explained by age was highest (1) with QSPECT, independently of the reference region, and (2) with whole brain as the reference, independently of the reconstruction algorithm.

Conclusion QSPECT reconstruction appears to be useful for reduction of camera-specific intersubject variability of [^{123}I]FP-CIT SPECT in multisite and single-site multicamera settings. Whole brain excluding striatal binding as the reference provides more stable quantitative estimates than occipital or cerebellar binding.

Keywords QSPECT · Dopamine transporter scintigraphy · [^{123}I]FP-CIT · Specific binding ratio · Age · ENC-DAT

Introduction

SPECT with the ligand *N*-ω-fluoropropyl-2β-carbomethoxy-3β-(4-[^{123}I]iodophenyl)nortropane ([^{123}I]FP-CIT, FP-CIT) for the presynaptic dopamine transporter (DAT) is widely used in the diagnostic process of parkinsonian syndromes and for the differentiation between Alzheimer's disease and dementia with Lewy bodies [1–5]. The interpretation of DAT SPECT is based on visual evaluation of the images which can be supported by quantitative analysis [6–12]. In some studies, quantitative analysis provided better diagnostic accuracy than visual rating. For example, O'Brien et al., evaluating FP-CIT SPECT for the differential diagnosis of dementia with Lewy bodies and Alzheimer's disease, found that quantitative analysis resulted in considerably better specificity than visual rating (94 % vs. 85 %) with equal sensitivity (78 %), although visual assessment was undertaken by five independent, trained raters [13]. This underlines the potential of quantitative analysis in FP-CIT SPECT.

However, in this single-centre study by O'Brien et al. all participants were scanned with the same SPECT camera and according to the same acquisition and reconstruction protocol [13]. It is well known that the SPECT equipment, including both hardware and software, has a significant impact on the reconstructed images. For ^{99m}Tc-labelled tracers the impact of camera hardware is rather small [14], so that the main contribution to camera-specific variability in ^{99m}Tc SPECT studies is due to vendor-specific differences in the reconstruction software. SPECT with ^{123}I-labelled tracers is sensitive also to hardware due to penetration of high-energy photons. Camera-specific variability in FP-CIT SPECT binding ratios has been demonstrated by Tossici-Bolt et al. who performed ^{123}I SPECT imaging of the same striatal phantom in 15 European centres on 17 SPECT systems and found a random variability in the quantitative analysis among the SPECT systems of up to 13.9 % [15].

The impact of SPECT system dependence on diagnostic accuracy is most likely more pronounced in quantitative analysis than in visual rating. This might explain the fact that, for example, the phase III multicentre trial of FP-CIT SPECT in dementia with Lewy bodies did not demonstrate diagnostic accuracy of quantitative analysis but of visual rating only [16].

The system dependence of quantitative analysis of FP-CIT SPECT can be reduced by applying the same reconstruction algorithm to scatter-compensated and penetration-compensated projection data, the latter being considered independent of the SPECT camera. This approach has been successfully implemented in a European multicentre study initiated by the Neuroimaging Committee of the European Association of Nuclear Medicine to generate a database of FP-CIT SPECT in healthy controls (ENC-DAT) [17]. The aim of this initiative was to provide reference images and values for quantitative analyses over a wide age range from young adolescence (20 years) to old age (90 years). SPECT images were reconstructed by a core laboratory using a LINK or HERMES workstation (see section Image reconstruction).

Analyses of ENC-DAT data have shown an age-related decline in the specific binding ratio (SBR) in the striatum and its subregions [17, 18]. The age effect was statistically highly significant, not least due to the large age range and the large sample size. However, there was strikingly large intersubject variability in SBR which could not be explained by age or any of the other covariates considered (gender, handedness, body mass index, and season and time of day when the FP-CIT SPECT was performed) [17, 18]. A considerable fraction of this still unexplained intersubject variability might be related to camera-specific intersite variability in the imaging process rather than being actual physiological variability in DAT availability, despite the efforts to minimize intersite variability.

The primary aim of the present study therefore was to reduce nonphysiological intrasite and intersite variability in FP-CIT SPECT scans in the ENC-DAT by the use of the reconstruction algorithm 'QSPECT', which is expected to be particularly useful in multisite settings. QSPECT is an OSEM reconstruction algorithm with (1) fully automated detection of the outer contour of the head for iterative reconstruction including attenuation correction, (2) correction for scatter and

septal penetration by transmission-dependent convolution subtraction (TDCS), and (3) "to kBq/ml" calibration of voxel intensities [19–21]. QSPECT explicitly accounts for the camera with which the SPECT data were acquired by using camera-specific calibration factors for correction of scatter and septal penetration as well as for "to kBq/ml" calibration. These camera-specific factors were measured previously and are available in the QSPECT software. QSPECT has been successfully used in multicentre studies of brain perfusion SPECT with [^{123}I]iodoamphetamine [22, 23].

We hypothesized that the use of QSPECT would reduce nonphysiological intersubject variability in quantitative measures of DAT availability in the ENC-DAT data compared to previous analyses. To test this hypothesis, the correlation between SBR and age was used as the primary quality measure (stronger correlation indicating a reduction in nonphysiological variability). A secondary aim of the study was to evaluate different reference regions for estimation of nonspecific FP-CIT binding with respect to their impact on the random error in the quantitative analysis.

Materials and methods

Subjects

Data from 73 healthy subjects recruited at six different centres were obtained from the European Normal Control Database of FP-CIT (ENC-DAT) [15, 17]. The centres were selected (1) to encompass a spectrum of SPECT systems currently in clinical use and (2) to include only data from SPECT cameras for which the camera-specific factors for correction of scatter and septal penetration were available in QSPECT (see section Image reconstruction). Inclusion and exclusion criteria of the ENC-DAT study have been described previously [17]. Three subjects from one centre (Amsterdam) were excluded from the present study because of serious truncation of their projection data. Details of the remaining 70 subjects are given in Table 1. Handedness was assessed using the Edinburgh Inventory [24]. However, handedness was not taken into account in the analyses of the present study because only seven subjects (10 %) were left-handed.

SPECT imaging

SPECT imaging was performed with six different cameras of various model types from two different manufacturers (Table 1). All cameras were equipped with low-energy high-resolution (LEHR) parallel-hole collimators. The cameras were certified prior to the start of subject recruitment. Their stability during the recruitment phase was verified by a rigorous quality control protocol [17]. Subject preparation

Table 1 [^{123}I]FP-CIT SPECT data of healthy subjects from the ENC-DAT included in the present study

Centre	SPECT camera	Acquisition time (h)	No. of subjects (male/female)	Handedness (right/left)	Body weight (kg), mean ± SD	FP-CIT dose (MBq), mean ± SD	Specific FP-CIT dose (MBq/kg body weight), mean ± SD (range)	Age (years), mean ± SD (range)
Munich	Siemens Symbia	3	14 (7/7)	11/3	76.2 ± 14.0	182 ± 4	2.47 ± 0.49 (1.78 – 3.54)	52 ± 17 (23 – 74)
Leuven	Siemens ECAM	3	15 (9/6)	14/1	73.1 ± 11.2	185 ± 4	2.59 ± 0.40 (2.01 – 3.48)	52 ± 18 (20 – 78)
Genoa	GE Millennium VG	3	14 (7/7)	13/1	71.0 ± 13.6	199 ± 15	2.90 ± 0.58 (2.05 – 3.96)	54 ± 19 (27 – 82)
London	GE Infinia Hawkeye 4	3	10 (6/4)	9/1	76.0 ± 9.7	177 ± 12	2.37 ± 0.40 (1.62 – 3.09)	61 ± 17 (25 – 78)
Amsterdam	Siemens ECAM	4	7 (3/4)	6/1	78.9 ± 11.7	186 ± 7	2.40 ± 0.38 (1.94 – 2.89)	63 ± 5 (56 – 70)
Ankara	GE Infinia GP4	3	10 (5/5)	10/0	73.1 ± 14.7	155 ± 11	2.20 ± 0.42 (1.69 – 3.00)	38 ± 16 (21 – 74)
All			70 (37/33)	63/7	74.3 ± 12.5	182 ± 16	2.52 ± 0.50 (1.62 – 3.96)	53 ± 18 (20 – 82)

and acquisition protocol have been described in detail previously [17]. In some subjects, two SPECT scans were acquired, one at 3 h the other at 4 h after injection. The present study included the 3-h scans except for the subjects from Amsterdam. In Amsterdam, a brain-dedicated SPECT system, Neurofocus, was used at 3 h after injection and a Siemens ECAM was used at 4 h after injection. The scans acquired on the ECAM at 4 h after injection were used in the present study, because the reconstruction method to be tested, QSPECT, did not allow processing of raw data acquired on the Neurofocus system, but can be applied to projection data from conventional SPECT systems only.

Image reconstruction

Transverse SPECT images generated from projection data using three different software packages were used in the present study. First, images reconstructed on a Link workstation with MAPS-10000 software (Link Medical) were obtained from the ENC-DAT (LINK method). LINK reconstruction was performed on projection data already corrected for scatter and septal penetration using the triple energy window technique [25, 26]. LINK reconstruction employed the original OSEM code by R. Larkin (Macquarie University code "R v2005.200 Mar 7 2005" [27]) with 10 iterations/10 subsets and 12 iterations/8 subsets for raw data with 120 and 128 projections, respectively [15, 17]. OSEM parameter settings differed from the default with respect to "Start-Image" and "DivRecon" as described previously [15]. Attenuation correction was performed iteratively based on ellipses of variable size with uniform (narrow beam) attenuation coefficient $\mu = 0.143\ cm^{-1}$ fed into OSEM [15]. The ellipses were defined automatically by contour finding based on background counts in the skull and were checked for accurate delineation of the head by visual inspection in each individual scan. A Butterworth filter with cut-off 0.50 cm^{-1} and order ten was used for three-dimensional postfiltering.

Second, reconstruction was performed on a Hermes workstation (Hermes Medical Solutions, Stockholm; HERMES method). Raw data were corrected for scatter and septal penetration using the same triple energy window technique as in the LINK method [25, 26]. Attenuation correction was performed by the iterative Chang technique using semiautomatically defined elliptical head outlines and a uniform (narrow beam) attenuation coefficient of $\mu = 0.143\ cm^{-1}$. HERMES used the same version of Larkin's OSEM code [27] as LINK, but with default settings for all parameters including "Start-Image" and "DivRecon". There were 10 iterations/10 subsets and 12 iterations/8 subsets for raw data with 120 and 128 projections, respectively. A Butterworth filter with cut-off 0.50 cm^{-1} and order ten was used for three-dimensional postfiltering [17].

Third, images were reconstructed using the QSPECT software package (QSPECT method). QSPECT first generates a uniform attenuation μ map by automated detection of the outer contour of the head. The latter is based on fitting sine-waves to the edges of the head in the sinogram representation of the projection data prior to scatter correction. Sinograms without scatter correction are used for this purpose, because photons scattered in the skull (or the scalp) are incorrectly located to the skull (or the scalp) and therefore tend to accentuate the edges of the head. This stabilizes the fit of the head contour and therefore allows more irregular shapes than ellipses in image space. QSPECT saves the attenuation μ map so that it can be checked for correct head delineation by visual inspection.

For scatter correction, QSPECT applies the TDCS method to generate scatter-free projection data on a geometric mean (GM) basis [28–30]. Geometric averaging of opposed projections halves the number of projections. Scatter correction is extended to account also for septal photon penetration [20], which is non-negligible in the case of ^{123}I particularly with low-energy (e.g. LEHR) collimators. Collimator-specific septal penetration factors were used, which have been measured previously. 'QSPECT OSEM' reconstruction was applied to the GM projections with 4 iterations/8 subsets (slice thickness 2 mm, pitch 1). QSPECT OSEM is an OSEM implementation independent of the Macquarie code. Differences between the two OSEM implementations include the collimator aperture modelling, the scatter function, and the offset to account for down scatter [20, 29]. QSPECT performs attenuation correction iteratively during reconstruction. A uniform attenuation map with $\mu = 0.160\ cm^{-1}$ inside the head contour was used as this value has been shown to provide the best agreement with attenuation correction based on transmission scanning in human brain [20]. A three-dimensional isotropic gaussian kernel with 7 mm full-width at half-maximum (FWHM) was used for postfiltering. This filter was selected based on a small pilot study using visual scoring of image quality by an experienced reader. Finally, reconstructed images were scaled by a previously measured camera-specific "to kBq/ml" calibration factor and taking into account voxel size, duration of the acquisition and the number of projections. This resulted in quantitative QSPECT images with voxel intensities representing the radioactivity concentration in kilobecquerels per millilitre [22, 23]. It should be noted that the calibration to "kBq/ml" did not affect the results of the present study, since any global calibration factor cancels in the computation of the SBR (see section Quantitative analysis).

Quantitative analysis

Regions of interest (ROIs) for the left and right striatum, whole brain, occipital lobe and cerebellum were positioned

manually for each individual subject. This individual ROI set could be used without any changes in all three SPECT images of the subject, i.e. with each reconstruction method, since the reconstructed field of view and voxel size (2.398 mm) were exactly the same for all reconstruction methods. Coregistration and/or reslicing of one image to another, which can introduce some bias due to additional smoothing during interpolation, or manual adaptation of the ROIs between the different reconstruction methods were not required. ROIs for the left and right striatum, whole brain and occipital lobe were defined in 18 consecutive transverse slices, left and right striatum by 'big' rectangles, and whole brain and occipital lobe by ellipses (Fig. 1). The volume of the unilateral striatum ROI was 127.6 ml. The cerebellum ROI was defined in six consecutive transverse slices through the cerebellum using an ellipse (Fig. 1). The number of slices was reduced if part of the cerebellum had not been within the field of view of the SPECT acquisition in order to avoid underestimation of the nondisplaceable FP-CIT binding by "air voxels" in the cerebellar ROI.

The SBR was computed according to the Southampton method developed by Fleming et al. to reduce the impact of recovery and partial volume effects [31]. More precisely, the SBR was computed according to the formulas:

$$SBR = SUSI/V_S, \quad (1)$$

where V_S is the volume of the striatum (assumed to be 11.2 ml), and the specific uptake size index (SUSI) is obtained as:

$$SUSI = (T - C_R{*}\ V)/C_R = T/C_R - V \quad (2)$$

where T is the total activity in the striatal ROI (in kilobecquerels), V is the volume of the striatal ROI (in millilitres) and C_R is the FP-CIT activity concentration in the reference region (in kilobecquerels/millilitre).

The two ROIs for the left and right striatum were much bigger than the actual striatal volume in order to guarantee that all striatal counts were included (despite spatial 'smearing' of striatal counts due to limited spatial resolution and residual anatomical intersubject variability after stereotactic normalization) but no other brain structure with FP-CIT binding uptake above background activity. The striatal ROIs were about the same size as described in the original paper (Fig. 1 of Fleming et al. [31]). The mean concentration of FP-CIT in the whole brain, without the striata, or in the occipital lobe or in the cerebellum was used as reference C_R. Combining each of the three reconstruction methods (LINK, HERMES, QSPECT) with each of the three reference regions (whole-brain without striata, occipital lobe, cerebellum) resulted in a total of nine different SBR values for (left or right) striatum in each subject.

Camera-specific recovery coefficients for the SBR have been determined by Tossici-Bolt et al. (ACSC recovery coefficients in Table I of Tossici-Bolt et al. [15]), but for LINK reconstruction only. As the recovery coefficients are expected to depend on the details of the reconstruction algorithm, even if all reconstructions include all corrections (attenuation, scatter and septal penetration), the reported recovery coefficients were not used in the present study in order to avoid bias to the disadvantage of HERMES and QSPECT.

Quantitative accuracy of QSPECT

The quantitative accuracy of QSPECT reconstruction, i.e. its accuracy in reproducing true tracer concentrations in kilobecquerels per millilitre, has been demonstrated by phantom measurements in a realistic three-dimensional brain phantom with bone and grey matter structures [32]. In the present study, the accuracy of QSPECT quantitative analysis in FP-CIT SPECT was evaluated. For this purpose, projection data from the striatal phantom measurements provided by the ENC-DAT [15] were reconstructed using QSPECT with exactly the same parameter settings as for human data, including camera-specific TDCS factors for correction of scatter and septal penetration, uniform attenuation coefficient ($\mu = 0.160\ cm^{-1}$), number of iterations (four) and subsets (eight), and gaussian postfiltering (FWHM 7 mm). Phantom

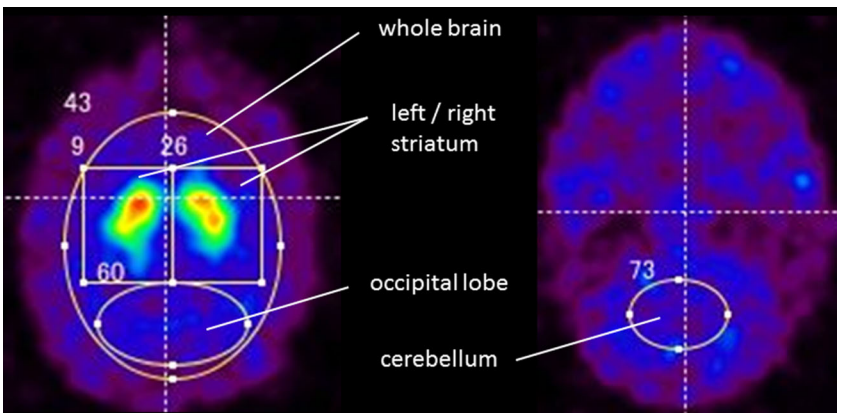

Fig. 1 Regions of interest

data were included from the same six ENC-DAT centres as in the analysis of human data. The SBR was obtained according to the Southampton method with the whole brain (without striata) as the reference as described above.

Statistical methods

Statistical analyses were performed with SPSS version 21 (IBM Corp., Armonk, NY). The mean of the left and right SBR was used in all analyses, since the mean showed a slightly better correlation with age than either the left or the right striatum separately, or the minimum over both hemispheres (the smallest left/right asymmetry of striatal SBR in ENC-DAT subjects, about 2 % larger in the left hemisphere [17], can be neglected in the present study). Univariate analysis of variance for repeated measures was performed to assess the impact of the reconstruction algorithm on the SBR. The effect of age on the SBR was tested by univariate analysis of variance with SBR as dependent variable, gender as random factor, and specific FP-CIT dose (i.e. injected dose in megabecquerels per kilogram body weight) and age as covariates. The rationale for including the specific FP-CIT dose in the model was that the SBR might be underestimated if statistical image quality is low associated with low specific FP-CIT dose. All values are presented as means ± 1 standard deviation of the sample. *P* values less than 0.05 were considered statistically significant.

Results

Results of the analysis of ENC-DAT striatal phantom data are summarized in Fig. 2. The true SBR was reproduced with an accuracy of ±5 % in almost all cases.

Orthogonal slices of the SPECT image of a representative human subject are shown in Fig. 3 for the three reconstruction algorithms. QSPECT reconstruction resulted in more homogeneous FP-CIT binding in extrastriatal brain regions compared with LINK and HERMES which both showed some 'fading out' of FP-CIT binding towards the edges of the brain (Fig. 3).

Analysis of variance for repeated measures with the reconstruction method as the intersubject factor revealed a highly significant effect of the reconstruction method on the SBR ($F = 584$, 137 and 91 for the whole brain without striata, occipital lobe and cerebellum as reference region, respectively; $p < 0.0005$ in all cases). HERMES reconstruction resulted in the highest SBR values. LINK and QSPECT resulted in SBR values which were 3.5 ± 5.4 % and 27.4 ± 8.4 % lower (whole brain without striata as the reference region). Bland-Altman plots are given in Fig. 4. The difference between QSPECT and both LINK and Hermes was more pronounced at large SBR than at low SBR, suggesting a multiplicative rather than an additive effect.

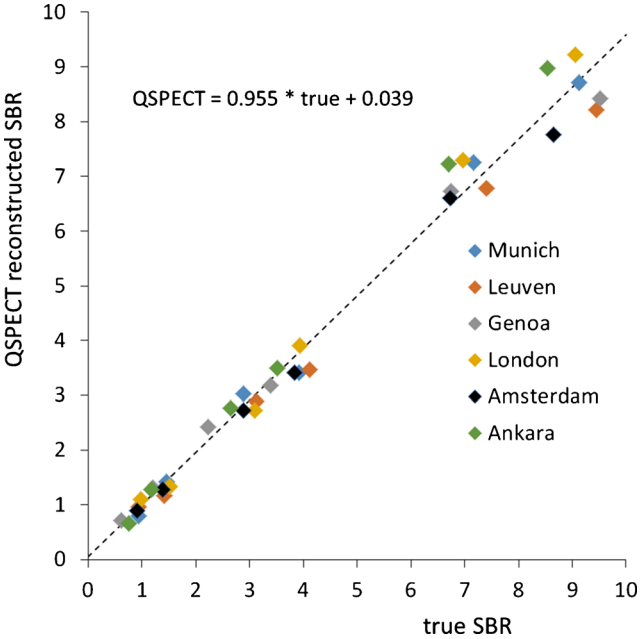

Fig. 2 ENC-DAT striatal phantom data. Southampton SBR (with whole brain without striata as reference) obtained from QSPECT reconstructed phantom images (with exactly the same parameter settings as in the human ENC-DAT data) plotted against the true SBR. The *dashed line* is the linear regression line including the data of all sites combined

Scatter plots of SBR versus age for the different reconstruction algorithms and reference regions are shown in Fig. 5. The effect of age on SBR was statistically highly significant, except when the cerebellum was used as the reference region (Table 2).

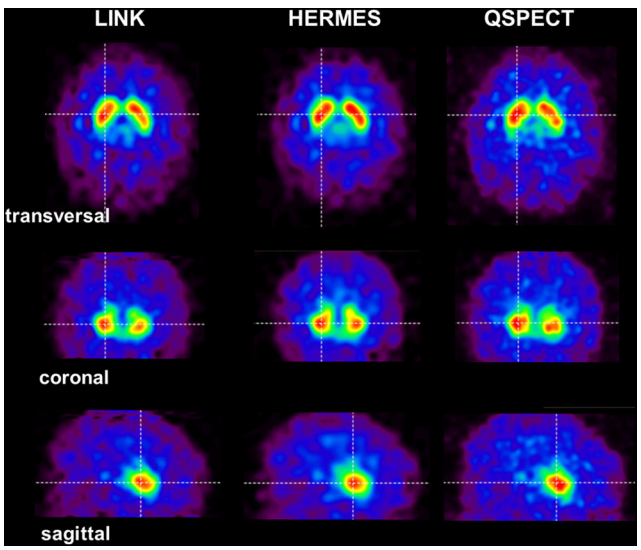

Fig. 3 Orthogonal slices of the [^{123}I]FP-CIT SPECT image in one representative subject (a 23-year-old woman) reconstructed with the three different reconstruction algorithms

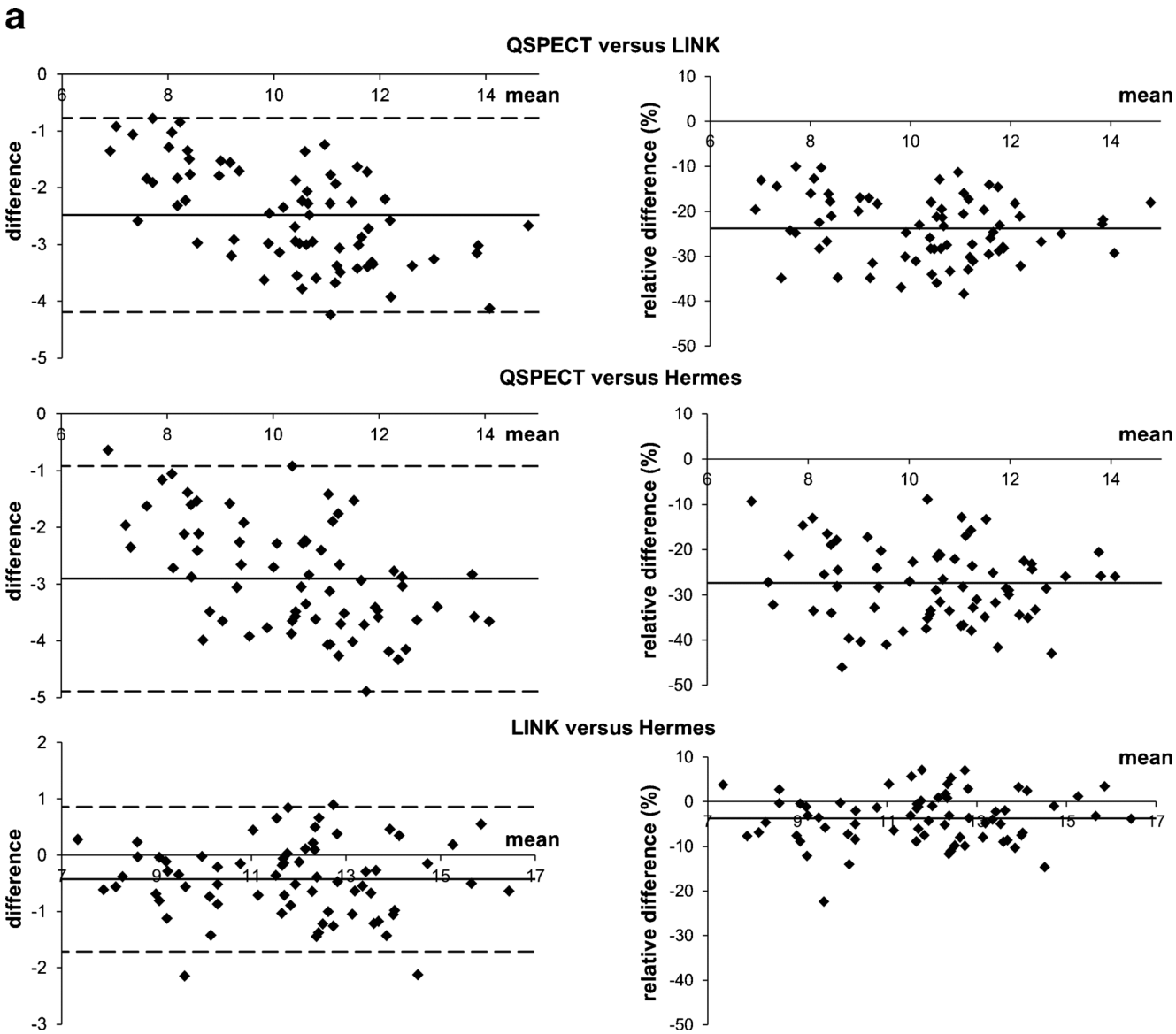

Fig. 4 **a** Bland-Altman plots of the specific FP-CIT binding ratio over all subjects for QSPECT versus LINK reconstruction (*top*), QSPECT versus Hermes reconstruction (*middle*) and LINK versus Hermes reconstruction (*bottom*) using the whole brain without striata as the reference region in all cases. **b** Bland-Altman plots of the specific FP-CIT binding ratio over all subjects for QSPECT versus LINK reconstruction using the whole brain without striata (*top*), occipital lobe (*middle*) and cerebellum (*bottom*) as the reference regions. *Left* absolute difference versus mean, *right* percentage difference (= 100 × difference/mean) versus mean

There was no significant effect of specific FP-CIT dose on SBR. This was confirmed by repeated univariate analysis of variance without specific FP-CIT dose in the model. For example, with QSPECT reconstruction and whole brain without striata as the reference, the (unstandardized) regression coefficient for the effect of age on SBR changed to −5.18 ($p = 0.000$; 95 % CI −6.94, −3.43) from −5.08 ($p = 0.000$; 95 % CI −6.82, −3.33) when the specific FP-CIT dose was included in the model (Table 2). The proportion of variance in the SBR explained by age changed to 0.341 from 0.339 (Table 2).

Concerning the impact of the reconstruction algorithm on the proportion of variance in the SBR explained by age, QSPECT reconstruction resulted in the highest proportion independently of the reference region (Table 2). With the whole brain without striata as the reference region, for example, age accounted for 33.9 % of the variance of SBR with QSPECT reconstruction, but only 25.9 % and 22.5 % with LINK and HERMES reconstruction, respectively. This was confirmed using the regression coefficients from the univariate analysis of variance to correct SBR for both age and specific dose (to the respective means of 53 years and 2.5 MBq/kg, respectively). The coefficient of variance (standard deviation/mean) of the corrected SBR was lowest for QSPECT (13.8 %)

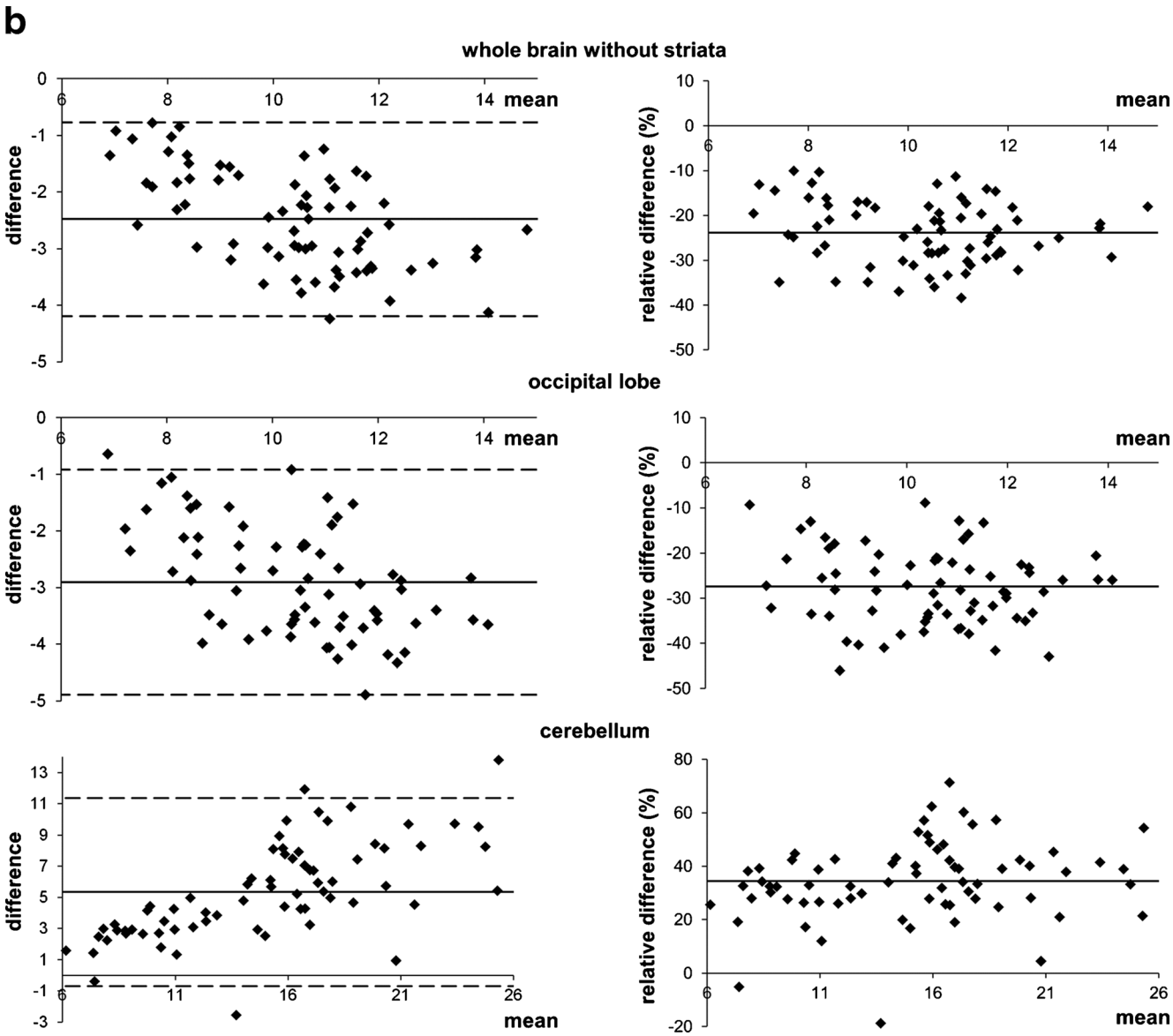

Fig. 4 continued.

and similar for LINK (15.3 %) and HERMES (15.0 %). The difference in the coefficient of variance was tested pair-wise for statistical significance using the Pitman test for comparison of variances in two paired samples [33]. The Pitman test consists of testing for correlation between the sum and the difference between paired observations (with a significant correlation indicating a significant difference in the variances). The nonparametric Spearman test revealed that the variance with QSPECT was significantly different from that with LINK (Spearman's rho = −0.247, $p = 0.039$), but was not significantly different from that with HERMES (rho = −0.142, $p = 0.242$). The difference in the variances between LINK and HERMES was also not significant (rho = 0.062, $p = 0.613$).

Concerning the impact of the reconstruction method on the age-associated decline in SBR, linear regression revealed the following regression line slopes:

For LINK: SBR = 14.8 – 0.606 × age/10
For HERMES: SBR = 15.0 – 0.568 × age/10
For QSPECT: SBR = 11.8 – 0.519 × age/10

(using the whole brain without striata as the reference region). Thus, in absolute terms, the slope was steepest for LINK and flattest for QSPECT. However, the percentage loss of SBR, averaged over the age range of the included subjects, i.e. 20 – 82 years, was 4.5 %, 4.1 % and 4.8 % with LINK, HERMES and QSPECT, respectively (note that the percentage loss depends on age, in contrast

Table 2 Univariate analysis of variance in the whole sample of 70 subjects with specific binding ratio as dependent variable, gender as random factor, and specific [^{123}I]FP-CIT dose and age as covariates

	LINK	HERMES	QSPECT
Whole brain without striata			
B (×100)	−5.93	−5.45	−5.08
p	0.000	0.000	0.000
95 % confidence interval	−8.40, −3.47	−7.94, −2.97	−6.82, −3.33
η^2	0.259	0.225	0.339
Occipital lobe			
B (×100)	−5.66	−4.38	−4.82
p	0.000	0.003	0.000
95 % confidence interval	−8.53, −2.79	−7.17, −1.60	−6.80, −2.84
η^2	0.190	0.130	0.264
Cerebellum			
B (×100)	−5.88	−3.75	−5.33
p	0.149	0.542	0.046
95 % confidence interval	−13.93, +2.16	−15.95, +8.46	−10.55, −0.11
η^2	0.031	0.006	0.059

B partial (unstandardized) regression coefficient for the age effect (for convenience, $B \times 100$ rather than *B*), η^2 proportion of variance in SBR explained by age

to the slope). Thus, in relative terms, the age-associated decline was most pronounced with QSPECT.

Discussion

The aim of this study was to compare QSPECT, LINK and HERMES reconstruction with respect to nonphysiological intersubject variability of the striatal FP-CIT SBR in the ENC-DAT database. Each of the three reconstruction methods involves the same steps: first, raw projection data are corrected for scatter and septal penetration, second, corrected raw data are reconstructed by OSEM with iterative Chang attenuation correction, and third, a three-dimensional postfilter is applied. The most relevant difference between the three methods is in the correction for scatter and septal penetration in the first step. LINK and HERMES reconstruction both use the triple energy window method for this purpose. QSPECT applies the TDCS method to generate scatter-free projection data on a GM basis. The latter means that opposed projections are averaged so that

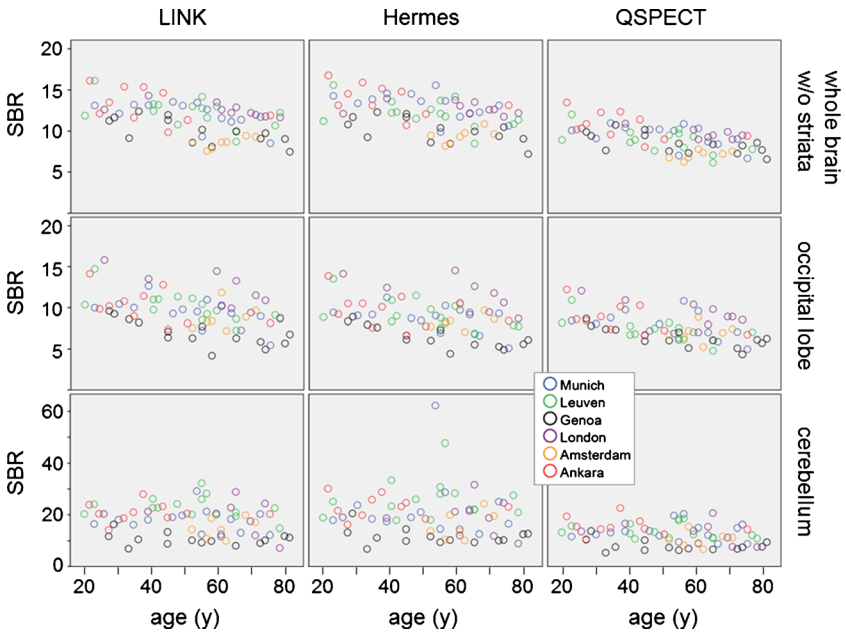

Fig. 5 Scatter plots of the specific FP-CIT binding ratio (SBR) versus age for the different reconstruction algorithms and reference regions. Note the difference in the scale of the *y*-axis for the cerebellum as reference region caused by increased variability and an outlier

the number of projections is halved. In QSPECT, the TDCS is adapted to also account for septal photon penetration, using collimator-specific septal penetration factors which have been measured previously. The TDCS avoids enhancement of statistical noise, in contrast to the triple energy window method which introduces additional noise through the subtraction of noisy scatter counts measured in additional, rather narrow energy windows [20]. Building the GM of opposed projections prior to TDCS provides further noise reduction in QSPECT.

Another difference lies in the detection of the head contour for Chang attenuation correction. LINK and HERMES both use ellipses to fit the outer contour of the head. QSPECT fits sine-waves to the edges of the head in the sinogram representation of the projection data prior to scatter correction. This allows more irregular shapes than ellipses in image space. Although the difference is small in most patients, it might not be completely negligible in some patients, in whom the more irregular shape provides potential for more accurate attenuation correction with QSPECT and, therefore, a reduction in intersubject variability associated with attenuation correction errors.

The primary hypothesis of the study was that QSPECT reduces nonphysiological intersubject variability of the striatal FP-CIT SBR in the ENC-DAT data compared with LINK and HERMES. To test this, the correlation between SBR and age was used as the primary quality measure (stronger correlation indicating a reduction in nonphysiological variability). In line with the primary hypothesis, the fraction of variability of the striatal FP-CIT SBR explained by age was largest with QSPECT reconstruction. After correction for age (and specific dose), the coefficient of variance of the SBR with QSPECT was lower than with both LINK (13.8 % versus 15.3 %, $p = 0.039$) and HERMES (15.0 %), although the latter difference did not reach statistical significance ($p = 0.242$). This suggests that QSPECT reconstruction allows a reduction in nonphysiological variability in FP-CIT SPECT SBR, including camera-specific intercentre variability. We hypothesize that camera-specific correction for scatter and septal penetration by QSPECT contributed to this improvement.

Concerning the magnitude of the reconstruction effect on intersubject variability, age accounted for 33.9 %, 25.9 % and 22.5 % of the SBR variance with QSPECT, LINK and HERMES, respectively (using the whole brain without striata as the reference region). The improvement with QSPECT, i.e. a reduction of unexplained variability of about 10 %, might appear rather small at first sight. However, the effect is large enough to immediately catch one's eye when inspecting the scatter plots of SBR versus age (Fig. 5). Furthermore, even a small reduction in errors in quantitative analysis may be relevant, because quantitative analysis might be most useful in borderline cases with a mild reduction in striatal FP-CIT uptake in which visual analysis requires a lot of expertise. However, in these borderline cases the decision is rather sensitive to small variations in the quantitative parameters, i.e. a small change might direct the interpretation as either reduced (neurodegenerative parkinsonism) or normal (non-neurodegenerative).

Varrone et al. [17] found reduced intersite variability in the ENC-DAT using camera-specific SBR recovery coefficients that had been measured with an anthropomorphic striatal phantom at each of the participating sites [15]. The phantom measurements demonstrated that there is variability not only across different SPECT models but also within different systems of the same model type, perhaps due to differences in crystal properties. Camera-specific SBR recovery coefficients were not used in the present study, because they were available for LINK reconstruction only. Camera-specific TDCS and "to kBq/ml" factors implemented in QSPECT are not specific to FP-CIT SPECT, but apply to all tracers (labelled with the same isotope), in contrast to the postreconstruction camera-specific SBR recovery coefficients, which are applicable to the SBR in FP-CIT SPECT only. Nevertheless, camera-specific SBR recovery coefficients might allow further reduction in unexplained SBR variance.

We hypothesize that the reduction in intersubject variability with QSPECT is also related to more homogeneous background binding across the whole brain (Fig. 3), which reduces intersubject variability of the nonspecific count concentration C_R. Homogenous background activity also simplifies visual interpretation of the SPECT images by improved anatomical delineation of the brain.

'Fading out' of nonspecific FP-CIT binding towards the edges of the brain with LINK and HERMES might also have resulted in underestimation of mean FP-CIT binding in whole brain (without striata) as the reference value, which in turn would explain why striatal SBR was on average about 25 % higher with LINK and HERMES than with QSPECT. The 25 % difference between QSPECT and LINK/HERMES SBR appears surprisingly large at first sight, particularly considering that both QSPECT (Fig. 2) and LINK [15] accurately reproduced the true SBR in a realistic, i.e. anthropomorphic, striatal phantom. To some extent this might be explained by the sensitivity of the Southampton method with respect to variation of C_R. The latter is associated with the large size of the striatum ROI typically used with the Southampton method to make sure that all striatal counts are collected in each individual subject. This can be seen as follows. The total tracer binding T in the (generous) striatum ROI can be written as the sum of striatal and extrastriatal counts:

$$T = V_S' * C_S + \left(V - V_S'\right) * C_R' \tag{3}$$

where V_S' is the actual volume of the striatum (that could be different from V_S), C_S is the FP-CIT concentration in the striatum, and C_R' is the (nondisplaceable) FP-CIT concentration in extrastriatal voxels within the striatum ROI (that could be

different from C_R). Inserting Eq. 3 into the definition of the Southampton SBR according to Eqs.. 1 and 2 results in:

$$SBR = \frac{V_S'}{V_S} * \frac{C_S - C_R'}{C_R} + \frac{V}{V_S} * \frac{C_R' - C_R}{C_R} \quad (4)$$

If $V_S' = V_S$ and $C_R' = C_R$, the first term in Eq. 4 is the true SBR, and the second term vanishes. If C_R slightly underestimates C_R', the first term is still a good approximation of the actual SBR. However, the second term becomes rather large, that is due to the amplification factor $V/V_S = 127.6\ \text{ml}/11.2\ \text{ml} = 11.4$. For example, in case of 10 % underestimation of C_R' ($C_R = 0.9 \times C_R'$), the second term computes to 1.3, i.e. SBR is overestimated by 1.3. For true SBR = 7, this accounts for an overestimation by 19 %. Thus, the difference in SBR observed between QSPECT and LINK/HERMES might be explained by a difference in C_R of about 10 %. This rather small difference might be explained by some extra factors when moving from a striatal phantom to patients, e.g. contribution of activity from distant body parts to scatter and septal penetration, for which QSPECT and LINK/HERMES correct differently.

According to Eq. 4, variation in C_R has an even bigger effect in cases of poor specific binding. For example, the relative SBR change caused by a 10 % C_R difference increases from 19 % for true SBR = 7, to 33 % for true SBR = 4, to 65 % for true SBR = 2, to 130 % for true SBR = 1. Yet this effect was not observed in the human data in this study: the percentage SBR difference between QSPECT and LINK/HERMES was more or less independent of the SBR (Fig. 4, right column). However, the ENC-DAT subjects cover only the range SBR ≥ 7 (Fig. 5) at which the C_R dependence of the SBR is rather flat. Studies including patients with reduced SBR are required to test whether the percentage difference between QSPECT and LINK/HERMES SBR increases with decreasing SBR which then would support the hypothesis that the SBR difference between QSPECT and LINK/HERMES is due to differences in the C_R estimate.

It is important to note that the C_R-mediated impact of the reconstruction method on SBR depends on the reference region, as was expected: whereas using the whole brain (excluding the striata) and the occipital lobe resulted in lower SBR with QSPECT compared to LINK/HERMES, using the cerebellum resulted in higher SBR with QSPECT (Fig. 4b). Furthermore, the impact of the 'fading out' of nonspecific FP-CIT binding towards the edges of the brain might be reduced by shrinking the reference region to avoid 'fading out' edges.

The Southampton SBR depends not only on the nonspecific FP-CIT concentration C_R as measured, i.e. an error-prone quantity, but also on the total activity T in the striatum ROI. From Eq. 2, which is symmetrical in T and $1/C_R$, it is evident that the Southampton SBR is as sensitive to variation in T as it is to variation in C_R.

The secondary aim of this study was to evaluate different reference regions for estimation of nonspecific FP-CIT binding with respect to their impact on the random error in the quantitative analysis. The results demonstrate that the whole brain without striata outperformed the occipital lobe and cerebellum in this respect. The proportion of variance in the SBR explained by age was largest with the whole brain, independently of the reconstruction method. The requirements for the reference region in FP-CIT SPECT are that it shows (1) only very low DAT concentration and (2) the same nonspecific FP-CIT uptake as the striatum. DAT density is very low in the cerebellum and all neocortical brain regions [34]. However, very often the reference region is restricted to the occipital lobe [7, 35] or the cerebellum [8]. This restriction to a smaller than necessary reference region might result in increased test–retest and intersubject variability of the SBR, not only due to increased statistical noise in C_R secondary to the lower number of counts (see Eq. 2), but also due to variability in the identification (delineation) of the reference region in each individual scan. The results of the present study suggest that the largest possible reference region for FP-CIT SPECT, the whole brain without striata, indeed stabilizes quantitative analysis. This is in agreement with recent findings by Kupitz et al. who compared the whole brain (without striata and the predominantly SERT-binding regions thalamus and brainstem) as the reference region in FP-CIT SPECT to the frontal and occipital lobes [36]. The use of the whole brain resulted in the highest area under the ROC curve of the SBR for differentiation between neurodegenerative and nonneurodegenerative parkinsonian syndrome. Whole brain without striata as reference region for FP-CIT SPECT was first proposed by Tossici-Bolt et al. who used a 44-mm thick transaxial slice centred at the highest striatal FP-CIT binding for quantitative analyses [11].

The whole-brain (without striata) reference region includes the cerebrospinal fluid (CSF) space of the lateral and third ventricle and some interhemispheric voxels (although the frontal horn of the lateral ventricle and third ventricle are excluded to a large extent in most patients due to the large striatum ROI used with the Southampton method; Fig. 1). This might limit the use of the whole brain as reference region in clinical patient care, since the CSF space can be strongly dilated in patients. However, the contribution of non-grey matter voxels might be reduced by using the 75th percentile of the voxel intensities in the whole-brain ROI rather than the mean to characterize nonspecific tracer binding [36]. The 75th percentile excludes CSF voxels, and, assuming tracer uptake to be higher in cortical grey matter than in white matter, it is also more representative of grey than of white matter. Finally, the 75th percentile might also account for lesions such as stroke, since even a large stroke probably alters the distribution of voxel intensities only below the 75th percentile so that the 75th percentile is not affected. The whole-brain (without

striata) reference region also includes white matter. This might appear a further limitation at first sight, but the 'big' striatum ROIs typically used with the Southampton method might contain about as much white matter as grey matter. Thus, a reference region comprising a similar mixture of white and grey matter might be more appropriate than a pure grey matter ROI. However, in practice this is probably not relevant, because FP-CIT uptake is very similar in cortical grey matter and white matter.

Concerning the cerebellum as reference region, it must be stated that in some patients (with hunched shoulders) it is difficult to achieve a small radius of rotation of the detectors if the cerebellum is to be included within the field of view. In these patients, spatial resolution (which requires a small rotation radius) is preferred over cerebellar acquisition. This invalidates the cerebellum as reference region to some extent, since it is strongly recommended that the same reference region be used in all subjects.

This study did not compare the reconstruction methods with respect to their impact on spatial resolution. At first sight, this appears relevant in the context of noise reduction by QSPECT, since noise reduction might be achieved by degradation of spatial resolution. There is indeed some smoothing inherent both in the geometric averaging of opposite projections and in the convolution associated with the TDSC scatter correction used by QSPECT. The number of OSEM iterations/subsets as well as the kernel used for postfiltering also have an effect on spatial resolution. In LINK and HERMES, OSEM was applied with 10 iterations/10 subsets and 12 iterations/8 subsets for raw data with 120 and 128 projections, respectively, so that the effective number of maximum likelihood expectation maximization (MLEM) iterations was about 100 (number of iterations times number of subsets). In QSPECT, OSEM was applied with 4 iterations/8 subsets, so that the effective number of MLEM iterations appears considerably lower, which might indicate 'under-iteration' with QSPECT. However, correction for scatter (and septal penetration) with QSPECT results in a scatter-free GM of opposing projections and therefore halves the number of projections prior to reconstruction. This, according to our experience, speeds up the convergence of iterative reconstruction by a factor of more than 2. Thus, the effective number of MLEM iterations of QSPECT with 4 iterations and 8 subsets of GM projections is probably rather close to 100, i.e. similar to LINK and HERMES. This assumption is supported by the fact that the striatal SBR computed from QSPECT images reconstructed with 8 subsets reaches a plateau at about 4 iterations, i.e. additional iterations do not change the SBR (results not shown).

Postfiltering had a large impact on the visual appearance of SPECT images, but its effect on striatal SBR was negligible. This is because SBR was computed according to the Southampton method, which was specifically designed to eliminate the impact of spatial resolution [31]. Therefore, the results and conclusions of the present study were most likely not affected by possible differences in spatial resolution between the tested reconstruction algorithms.

Finally, ROIs for the quantitative analysis were placed manually in this study. It is possible to embed ROI definition in software for fully automated quantitative analysis of FP-CIT SPECT. However, the Southampton method uses large ROIs (Fig. 1), in contrast to conventional methods that use small ROIs which are intended to precisely delineate the anatomical structure of the striatum. Therefore, the Southampton method is less sensitive to the limitations of manual ROI placement.

In conclusion, both image reconstruction and the reference region have a considerable impact on intersubject variability of quantitative estimates of striatal DAT availability in FP-CIT SPECT. Among the tested software packages (all with correction for scatter and septal penetration, iterative Chang attenuation correction and OSEM reconstruction), QSPECT provided the lowest intersubject variability of the specific striatal FP-CIT binding ratio in healthy subjects from the ENC-DAT. Concerning the reference region, the whole brain excluding striata resulted in more stable results than either the occipital lobe or cerebellum, independent of the reconstruction algorithm, and therefore might be recommended as the reference region in FP-CIT SPECT.

Authors' contributions All authors made substantial contributions to the conception of the study, analysis of the data, and/or interpretation of the results. R.B. drafted the manuscript, and all other authors revised it critically for important intellectual content. All authors read and approved the final manuscript.

Compliance with ethical standards

Conflicts of interest R.B. received an honorarium from ABX-CRO for independent statistical analysis, interpretation of results, and drafting the manuscript. ABX-CRO collaborates in development and distribution of the QSPECT software package, developed by H.I. J.B. is a consultant at GE Healthcare.

Ethical approval All procedures performed in studies involving human participants were in accordance with the ethical standards of the institutional and/or national research committee and with the principles of the 1964 Declaration of Helsinki and its later amendments or comparable ethical standards.

Informed consent As the present study was retrospective in nature, formal consent was not required.

References

1. Booij J, Speelman JD, Horstink MW, Wolters EC. The clinical benefit of imaging striatal dopamine transporters with [123I]FP-CIT SPET in differentiating patients with presynaptic parkinsonism from those with other forms of parkinsonism. Eur J Nucl Med. 2001;28:266–72.

2. Booij J, Tissingh G, Boer GJ, Speelman JD, Stoof JC, Janssen AG, et al. [123I]FP-CIT SPECT shows a pronounced decline of striatal dopamine transporter labelling in early and advanced Parkinson's disease. J Neurol Neurosurg Psychiatry. 1997;62:133–40.
3. Tatsch K, Poepperl G. Nigrostriatal dopamine terminal imaging with dopamine transporter SPECT: an update. J Nucl Med. 2013;54:1331–8. doi:10.2967/jnumed.112.105379.
4. Van Laere K, Everaert L, Annemans L, Gonce M, Vandenberghe W, Vander Borght T. The cost effectiveness of 123I-FP-CIT SPECT imaging in patients with an uncertain clinical diagnosis of parkinsonism. Eur J Nucl Med Mol Imaging. 2008;35:1367–76. doi:10.1007/s00259-008-0777-2.
5. Walker Z, Costa DC, Walker RW, Shaw K, Gacinovic S, Stevens T, et al. Differentiation of dementia with Lewy bodies from Alzheimer's disease using a dopaminergic presynaptic ligand. J Neurol Neurosurg Psychiatry. 2002;73:134–40.
6. Booij J, Habraken JB, Bergmans P, Tissingh G, Winogrodzka A, Wolters EC, et al. Imaging of dopamine transporters with iodine-123-FP-CIT SPECT in healthy controls and patients with Parkinson's disease. J Nucl Med. 1998;39:1879–84.
7. Darcourt J, Booij J, Tatsch K, Varrone A, Vander Borght T, Kapucu OL, et al. EANM procedure guidelines for brain neurotransmission SPECT using (123)I-labelled dopamine transporter ligands, version 2. Eur J Nucl Med Mol Imaging. 2010;37:443–50. doi:10.1007/s00259-009-1267-x.
8. Koch W, Radau PE, Hamann C, Tatsch K. Clinical testing of an optimized software solution for an automated, observer-independent evaluation of dopamine transporter SPECT studies. J Nucl Med. 2005;46:1109–18.
9. Soderlund TA, Dickson JC, Prvulovich E, Ben-Haim S, Kemp P, Booij J, et al. Value of semiquantitative analysis for clinical reporting of 123I-2-beta-carbomethoxy-3beta-(4-iodophenyl)-N-(3-fluoropropyl)nortropane SPECT studies. J Nucl Med. 2013;54:714–22. doi:10.2967/jnumed.112.110106.
10. Tatsch K, Poepperl G. Quantitative approaches to dopaminergic brain imaging. Q J Nucl Med Mol Imaging. 2012;56:27–38.
11. Tossici-Bolt L, Hoffmann SM, Kemp PM, Mehta RL, Fleming JS. Quantification of [123I]FP-CIT SPECT brain images: an accurate technique for measurement of the specific binding ratio. Eur J Nucl Med Mol Imaging. 2006;33:1491–9. doi:10.1007/s00259-006-0155-x.
12. Zubal IG, Early M, Yuan O, Jennings D, Marek K, Seibyl JP. Optimized, automated striatal uptake analysis applied to SPECT brain scans of Parkinson's disease patients. J Nucl Med. 2007;48:857–64. doi:10.2967/jnumed.106.037432.
13. O'Brien JT, Colloby S, Fenwick J, Williams ED, Firbank M, Burn D, et al. Dopamine transporter loss visualized with FP-CIT SPECT in the differential diagnosis of dementia with Lewy bodies. Arch Neurol. 2004;61:919–25. doi:10.1001/archneur.61.6.919.
14. Graham LS, Fahey FH, Madsen MT, van Aswegen A, Yester MV. Quantitation of SPECT performance: Report of Task Group 4, Nuclear Medicine Committee. Med Phys. 1995;22:401–9.
15. Tossici-Bolt L, Dickson JC, Sera T, de Nijs R, Bagnara MC, Jonsson C, et al. Calibration of gamma camera systems for a multicentre European 123I-FP-CIT SPECT normal database. Eur J Nucl Med Mol Imaging. 2011;38:1529–40. doi:10.1007/s00259-011-1801-5.
16. McKeith I, O'Brien J, Walker Z, Tatsch K, Booij J, Darcourt J, et al. Sensitivity and specificity of dopamine transporter imaging with 123I-FP-CIT SPECT in dementia with Lewy bodies: a phase III, multicentre study. Lancet Neurol. 2007;6:305–13. doi:10.1016/S1474-4422(07)70057-1.
17. Varrone A, Dickson JC, Tossici-Bolt L, Sera T, Asenbaum S, Booij J, et al. European multicentre database of healthy controls for [123I]FP-CIT SPECT (ENC-DAT): age-related effects, gender differences and evaluation of different methods of analysis. Eur J Nucl Med Mol Imaging. 2013;40:213–27. doi:10.1007/s00259-012-2276-8.
18. Nobili F, Naseri M, De Carli F, Asenbaum S, Booij J, Darcourt J, et al. Automatic semi-quantification of [123I]FP-CIT SPECT scans in healthy volunteers using BasGan version 2: results from the ENC-DAT database. Eur J Nucl Med Mol Imaging. 2013;40:565–73. doi:10.1007/s00259-012-2304-8.
19. Iida H, Eberl S. Quantitative assessment of regional myocardial blood flow with thallium-201 and SPECT. J Nucl Cardiol. 1998;5:313–31.
20. Iida H, Narita Y, Kado H, Kashikura A, Sugawara S, Shoji Y, et al. Effects of scatter and attenuation correction on quantitative assessment of regional cerebral blood flow with SPECT. J Nucl Med. 1998;39:181–9.
21. Kim K, Watabe H, Shidahara M, Ishida Y, Iida H. SPECT collimator dependency of scatter and validation of transmission-dependent scatter compensation methodologies. IEEE Trans Nucl Sci. 2001;48:689–96.
22. Iida H, Nakagawara J, Hayashida K, Fukushima K, Watabe H, Koshino K, et al. Multicenter evaluation of a standardized protocol for rest and acetazolamide cerebral blood flow assessment using a quantitative SPECT reconstruction program and split-dose 123I-iodoamphetamine. J Nucl Med. 2010;51:1624–31. doi:10.2967/jnumed.110.078352.
23. Yoneda H, Shirao S, Koizumi H, Oka F, Ishihara H, Ichiro K, et al. Reproducibility of cerebral blood flow assessment using a quantitative SPECT reconstruction program and split-dose 123I-iodoamphetamine in institutions with different γ-cameras and collimators. J Cereb Blood Flow Metab. 2012;32:1757–64. doi:10.1038/jcbfm.2012.67.
24. Oldfield RC. The assessment and analysis of handedness: the Edinburgh inventory. Neuropsychologia. 1971;9:97–113.
25. Ichihara T, Ogawa K, Motomura N, Kubo A, Hashimoto S. Compton scatter compensation using the triple-energy window method for single- and dual-isotope SPECT. J Nucl Med. 1993;34:2216–21.
26. Ogawa K, Harata Y, Ichihara T, Kubo A, Hashimoto S. A practical method for position-dependent Compton-scatter correction in single photon emission CT. IEEE Trans Med Imaging. 1991;10:408–12. doi:10.1109/42.97591.
27. Hudson HM, Larkin RS. Accelerated image reconstruction using ordered subsets of projection data. IEEE Trans Med Imaging. 1994;13:601–9.
28. Meikle SR, Hutton BF, Bailey DL. A transmission-dependent method for scatter correction in SPECT. J Nucl Med. 1994;35:360–7.
29. Narita Y, Eberl S, Iida H, Hutton BF, Braun M, Nakamura T, et al. Monte Carlo and experimental evaluation of accuracy and noise properties of two scatter correction methods for SPECT. Phys Med Biol. 1996;41:2481–96.
30. Iida H, Shoji Y, Sugawara S, Kinoshita T, Tamura Y, Narita Y, et al. Design and experimental validation of a quantitative myocardial 201Tl SPECT system. IEEE Trans Nucl Sci. 1999;46:720–6.
31. Fleming JS, Bolt L, Stratford JS, Kemp PM. The specific uptake size index for quantifying radiopharmaceutical uptake. Phys Med Biol. 2004;49:N227–34.
32. Iida H, Hori Y, Ishida K, Imabayashi E, Matsuda H, Takahashi M, et al. Three-dimensional brain phantom containing bone and grey matter structures with a realistic head contour. Ann Nucl Med. 2013;27:25–36. doi:10.1007/s12149-012-0655-7.
33. Armitage P, Berry G. Statistical methods in medical research. 3rd ed. Oxford: Blackwell Science; 1994.
34. Hall H, Halldin C, Guilloteau D, Chalon S, Emond P, Besnard J, et al. Visualization of the dopamine transporter in the human brain postmortem with the new selective ligand [125I]PE2I. Neuroimage. 1999;9:108–16.

35. Djang DS, Janssen MJ, Bohnen N, Booij J, Henderson TA, Herholz K, et al. SNM practice guideline for dopamine transporter imaging with 123I-ioflupane SPECT 1.0. J Nucl Med. 2012;53:154–63. doi: 10.2967/jnumed.111.100784.

36. Kupitz D, Apostolova I, Lange C, Ulrich G, Amthauer H, Brenner W, et al. Global scaling for semi-quantitative analysis in FP-CIT SPECT. Nuklearmedizin. 2014;53:234–41. doi:10.3413/Nukmed-0659-14-04.